



OPEN ACCESS

EDITED BY

Yingjun Wu,
Hohai University, China

REVIEWED BY

Jiawei Wang,
Technical University of Denmark, Denmark
Zhengmao Li,
Aalto University, Finland
Dan Wang,
Tianjin University, China

*CORRESPONDENCE

Dongxu Zhou,
✉ zdx2001@163.com

RECEIVED 06 May 2024

ACCEPTED 16 August 2024

PUBLISHED 29 August 2024

CITATION

Zhou D, Xu J, Zhang C, Wei P, Pan G and Gu Z (2024) A multi-agent optimal operation methodology of electric, thermal, and hydrogen integrated energy system based on ADMM algorithm.
Front. Energy Res. 12:1428303.
doi: 10.3389/fenrg.2024.1428303

COPYRIGHT

© 2024 Zhou, Xu, Zhang, Wei, Pan and Gu. This is an open-access article distributed under the terms of the [Creative Commons Attribution License \(CC BY\)](https://creativecommons.org/licenses/by/4.0/). The use, distribution or reproduction in other forums is permitted, provided the original author(s) and the copyright owner(s) are credited and that the original publication in this journal is cited, in accordance with accepted academic practice. No use, distribution or reproduction is permitted which does not comply with these terms.

A multi-agent optimal operation methodology of electric, thermal, and hydrogen integrated energy system based on ADMM algorithm

Dongxu Zhou^{1*}, Jingzhou Xu¹, Can Zhang¹, Pengchao Wei¹, Guangsheng Pan² and Zhongfan Gu²

¹State Grid Nanjing Power Supply Company, Information and Communication Branch, Nanjing, China,

²School of Electrical Engineering, Southeast University, Nanjing, China

This article presents a study on the distributed optimization operation method for micro-energy grid clusters within an electric, thermal, and hydrogen integrated energy system. The research focuses on precisely modeling the Power-to-Hydrogen (P2H) conversion process in electrolytic cells by considering their startup characteristics. An optimization operation model is established, with each micro-energy grid as the principal entity, to cater to their individual interests and demands. The Alternating Direction Method of Multipliers (ADMM) algorithm is adopted for distributed solution. Case studies demonstrate that the connection topology between micro-energy grids significantly impacts the total operating cost, and the effectiveness of the ADMM algorithm is validated through a comparison with centralized optimization approaches.

KEYWORDS

power-to-hydrogen, integrated energy system, multi-agent optimal operation, alternating direction method of multipliers, electrolytic hydrogen

1 Introduction

By 2050, the projected increment in CO₂ emissions could span from 2.21 to 7.43 megatons, underscoring the urgency for decisive action. Amidst this backdrop, numerous nations worldwide have set forth ambitious carbon reduction targets, signaling a global commitment to mitigate climate change (Jiang et al., 2024). The Integrated Energy System (IES), a holistic approach that integrates power-to-heat conversion technologies and seamlessly intertwines heat and power generation, has emerged as a cornerstone in the pursuit of carbon emission reduction. This system, bolstered by its unique technological prowess, offers a pivotal pathway towards a greener future (Zhang et al., 2024).

The strategic deployment of complementary technologies within the IES framework further enhances renewable energy utilization, thereby mitigating adverse climate impacts (Pan et al., 2021). Among these, Power-to-Hydrogen (P2H) technology stands out as a highly efficient energy conversion mechanism, transforming electrical energy into hydrogen energy—a clean and versatile fuel source (Gu et al., 2024). As renewable energy capacity expands and electric vehicles, alongside other power-hungry devices, gain widespread adoption, the challenge of effectively managing surplus electricity has become paramount in the energy sector. P2H technology adeptly addresses this challenge by electrolyzing water, converting excess electrical energy into hydrogen, thereby not only alleviating the issue of surplus electricity but also

supplying a clean, green energy source for innovative applications like hydrogen-fueled vehicles. Moreover, P2H technology boasts several advantages that make it an attractive option for energy storage and conversion. Its high energy storage efficiency, prolonged storage capability, and zero-emission profile position it as a promising contender in the quest for sustainable energy solutions (Zhuang et al., 2023). By harnessing the full potential of both the IES and P2H technology, we can accelerate our transition towards a low-carbon, environmentally friendly future.

(He et al., 2021) proposes an integrated energy system optimization model that utilizes P2H technology to convert excess wind power into hydrogen, mitigating curtailment and filling load valleys. Case studies validate the effectiveness of this approach. Author in (Gu et al., 2023) propose a regional joint electrolytic hydrogen system framework to address differentiated electrolytic hydrogen capacity caused by resource characteristics in China. They established a decoupling model for cascade hydropower and compared its advantages over separate systems in terms of reducing hydrogen costs, carbon emissions, and renewable energy capacity. Differential models for electrolyzers were also established, providing insights into their evolution and development prospects (Gupta et al., 2023). studies the integration of P2H technology into utility-scale hybrid power plants (HPPs) consisting of wind, solar, and battery storage. As renewable energy resources and sector coupling increase, HPPs are evolving to include other energy vectors like heat and gas storage. Integrating P2H within HPPs reduces fluctuations from non-dispatchable production and curtailment, similar to storage devices. Case studies in Europe demonstrate the significant techno-economic benefits of HPPs with P2H. In (Zhao et al., 2022), the Integrated Energy Production Unit (IEPU) concept, combining P2H and Carbon Capture, Utilization, and Storage (CCUS) technologies, is proposed. This concept leverages existing synchronous turbines to provide synthetic active and reactive capabilities, validated using open-source software with European load data, optimizing capacity and simulating 8,760-h operations to minimize annual costs. In (Dong et al., 2023), the authors compare the technical characteristics of alkaline electrolyzers (AEC) and proton exchange membrane electrolyzers (PEMEC), and proposes an optimal planning model for P2H clusters. The model aims to minimize investment, operational, startup/shutdown, grid power purchase, network loss, and voltage deviation costs. A modified IEEE 33-node network case verifies the model's effectiveness and benefits (Lu et al., 2022). introduces an Approximate Dynamic Programming (ADP) method for optimizing real-time micro-energy grid operation with P2H devices. The ADP approach, leveraging a piecewise linear function, finds near-optimal strategies that adapt to uncertainties, outperforming Model Predictive Control (MPC) in case studies. Authors in (Cao et al., 2022) propose a dual-fuel cells hydrogen energy storage integrated energy system to enhance performance. Optimizing device capacities based on economic factors reveals an optimal configuration that outperforms single fuel cells. Sensitivity analysis highlights the influence of electricity, natural gas prices, and renewable energy capacity on the optimal hydrogen storage and fuel cell configuration.

However, a significant oversight in existing research lies in the neglect of electrolytic cells' start-up characteristics, notably the start-up delay and power requirements. While these cells are indispensable in converting renewable energy sources into hydrogen via the Power-to-Hydrogen (P2H) process, their initial operational phases, particularly the intricate start-up process, have remained largely unexamined. This oversight results in a lack of

granularity in electrolytic cell models, which in turn fails to accurately mirror the system's true operational dynamics. This uncharted territory represents a crucial gap that necessitates urgent attention and further exploration. Such endeavors would not only refine our understanding of these systems but also propel us closer to a greener, more sustainable future by ensuring that P2H technologies operate at their optimal capacity.

The Alternating Direction Method of Multipliers (ADMM) algorithm, renowned for its prowess in tackling optimization challenges, stands out as a formidable tool for resolving large-scale, decentralized, and intricate constraint optimization problems within the energy sector. Its unparalleled advantages have fostered widespread adoption in energy optimization applications. By masterfully decomposing intricate energy systems into manageable subproblems and iteratively solving them in an alternating fashion, the ADMM algorithm drastically reduces problem complexity and computational overhead. Moreover, its inherent distributed nature harmoniously aligns with the decentralized characteristics of energy systems, enabling seamless distributed optimization management, thereby enhancing overall system efficiency and performance.

(Huang et al., 2023) proposes a blockchain-based distributed market framework for the bi-level carbon and energy trading between coal mine integrated energy systems and a virtual power plant (VPP). (Kong et al., 2020) introduces a distributed optimization approach for integrated energy systems (IES) using the ADMM. The method begins by analyzing uncertain factors from energy sources and loads, employing scenario analysis to capture their stochasticity. An optimal scheduling model for IES is then formulated. Leveraging ADMM, this model is reformulated to enable distributed optimization for multi-energy complementation. Case study results demonstrate the effectiveness and practicality of the proposed strategy. Authors in (Chen et al., 2018) propose an enhanced energy hub (EH) model for IES, incorporating electric and heat energy storage along with solar thermal collectors. The IES is structured as a multi-operator system, with each EH belonging to a distinct operator. A distributed energy management model accounts for storage operation costs and shows effectiveness in reducing energy bills, transmission losses, and prolonging energy storage life. (Pan et al., 2022) offers a distributed operation strategy using an enhanced ADMM. It establishes models for gas turbines and energy storage, incorporating dynamic characteristics of radial distribution and natural gas networks. An optimization model for day-ahead scheduling reduces operating costs while managing renewable energy uncertainty through chance constraints. An ADMM-based distributed operation method with adaptive step size addresses information opacity between electricity and gas systems. (Wu et al., 2021) addresses the challenges of centralized control in large-scale integrated energy parks by proposing a distributed computing method. The method decomposes joint scheduling into subproblems, considers the coupling of electricity, gas, and heat, and establishes a day-ahead scheduling model. A case study demonstrates the feasibility of the distributed optimization model. Authors in (Li et al., 2024) propose an optimal operation strategy with dynamic partitioning for centralized shared energy storage stations, considering day-ahead demands of renewable energy power plants. A multi-entity cooperative optimization model based on Nash bargaining theory is implemented and decomposed into subproblems solved by ADMM. Simulations show improved tracking of renewable energy output, higher energy storage utilization, and increased profits for each entity.

In this article, we delve into a comprehensive study exploring the distributed optimization operation methodology for clusters of micro-energy grids within a multifaceted energy system that integrates electricity, heat, and hydrogen resources. Our research meticulously models the intricate Power-to-Hydrogen (P2H) conversion process within electrolytic cells, meticulously accounting for their nuanced startup dynamics. This nuanced approach ensures a precise portrayal of the P2H process, pivotal for optimizing the holistic energy system's performance. To this end, we formulate an optimization framework that recognizes each micro-energy grid as an autonomous entity, respecting their distinct interests and operational imperatives. This model not only considers the efficiency of energy conversion but also the specific operational constraints and goals of each micro-energy grid. To tackle this intricate distributed optimization challenge, we harness the power of the Alternating Direction Method of Multipliers (ADMM) algorithm, renowned for its prowess in handling large-scale, decentralized optimization problems. By utilizing ADMM, we can decompose the overall optimization problem into smaller subproblems, which are then solved iteratively in a distributed manner. This approach not only reduces the computational complexity but also enables each micro-energy grid to operate independently while still contributing to the overall optimization of the entire energy system.

2 P2H module unified operation model

2.1 Introduction for P2H technologies

In the commercial landscape of hydrogen production equipment, the electrolytic cell stack stands as the cornerstone unit. Nevertheless, the inherent power limitations of a solitary stack, often constrained to below 10 kW, underscore the need for scalability. By harnessing the inherent scalability of electrolytic cell technology, we can orchestrate multiple stacks into formidable modules, capable of achieving capacities that soar from 100 kW to the megawatt realm. The extensive hydrogen production systems utilized in power systems often comprise numerous independently managed modules, where each module can be selectively activated, deactivated, and its output precisely controlled. Therefore, this paper focuses its modeling and selection planning efforts on the electric hydrogen production module as the fundamental research subject.

2.2 Startup model of P2H modules

When initiating the P2H process, the start-up delay associated with low-temperature electrolysis technologies, such as AEC and PEMEC, tends to be minimal. However, in the case of SOEC utilizing high-temperature electrolysis, hydrogen gas production does not commence until the stack has reached a specific temperature threshold. Notably, the heating duration required to attain this temperature can often be significant and should not be overlooked.

In the context of the given modeling, i , k , and t represent distinct indices: i signifies the i -th micro energy grid, k denotes the k -th electrolytic cell, and t represents the time instant. The variable α_{EC}^k captures the startup delay specific to the k -th electrolytic cell. The

variable $x_{EC}^{i,k,t}$ represents the state of the k -th electrolytic cell within the i -th micro-energy grid at time t . Furthermore, $y_{EC}^{i,k,t}$ and $z_{EC}^{i,k,t}$ represent the start and stop actions, respectively, of the k -th electrolytic cell in the i -th micro-energy grid at time t . These actions indicate whether the electrolytic cell is being initiated or terminated at a given time.

The modeling of these variables allows for a comprehensive representation of the dynamic behavior and operational decisions within the integrated energy system.

The operating power of the EC is subject to upper and lower limits, which are mathematically constrained as expressed in Equation 1. This constraint ensures that the electrolytic cell operates within its safe and efficient range, preventing over- or under-utilization.

$$x_{EC}^{i,k,t} \cdot \delta_{EC,in,1,\min}^{i,k} \cdot Cap_{EC}^{i,k} \leq P_{EC,in,1}^{i,k,t} \leq x_{EC}^{i,k,t} \cdot \delta_{EC,in,1,\max}^{i,k} \cdot Cap_{EC}^{i,k} \quad (1)$$

where $P_{EC,in,1}^{i,k,t}$ represents the EC input power that is utilized for hydrogen production (output). This is the active power input that drives the electrolysis process and generates hydrogen gas. $Cap_{EC}^{i,k}$ represents the installed capacity of the EC. $\delta_{EC,in,1,\min}^{i,k} / \delta_{EC,in,1,\max}^{i,k}$ represents the ratio of the minimum/maximum value of $P_{EC,in,1}^{i,k,t}$ to the installed capacity.

The starting power constraint of EC is shown in Equation 2.

$$P_{EC,in,2}^{i,k,t} = \sum_{\tau=0}^{\alpha_{EC}^k-1} y_{EC}^{i,k,t-\tau} \cdot \delta_{EC,boot}^{i,k} \cdot Cap_{EC}^{i,k} \quad (2)$$

where $P_{EC,in,2}^{i,k,t}$ represents the EC input power used specifically for starting the electrolytic cell. This power is consumed only during the startup phase and does not contribute to hydrogen production. It is typically required to heat the stack and other components to the operating temperature. $\delta_{EC,boot}^{i,k}$ represents the ratio of the starting power $P_{EC,in,2}^{i,k,t}$ to the installed capacity.

The state constraints of EC are shown in Equation 3.

$$\begin{aligned} y_{EC}^{i,k,t-\alpha_{EC}^k} - z_{EC}^{i,k,t} &= x_{EC}^{i,k,t} - x_{EC}^{i,k,t-1} \\ y_{EC}^{i,k,t} &\leq 1 - x_{EC}^{i,k,t-1} \\ z_{EC}^{i,k,t} &\leq x_{EC}^{i,k,t-1} \end{aligned} \quad (3)$$

In Equation 3, the first equation represents the constraints imposed by the start-up and shutdown action variables on the state variables of the electrolytic cell. The second equation indicates that the electrolytic cell can only be started when it is in the off state, while the third equation indicates that the electrolytic cell can only be shut down when it is in the start-up state.

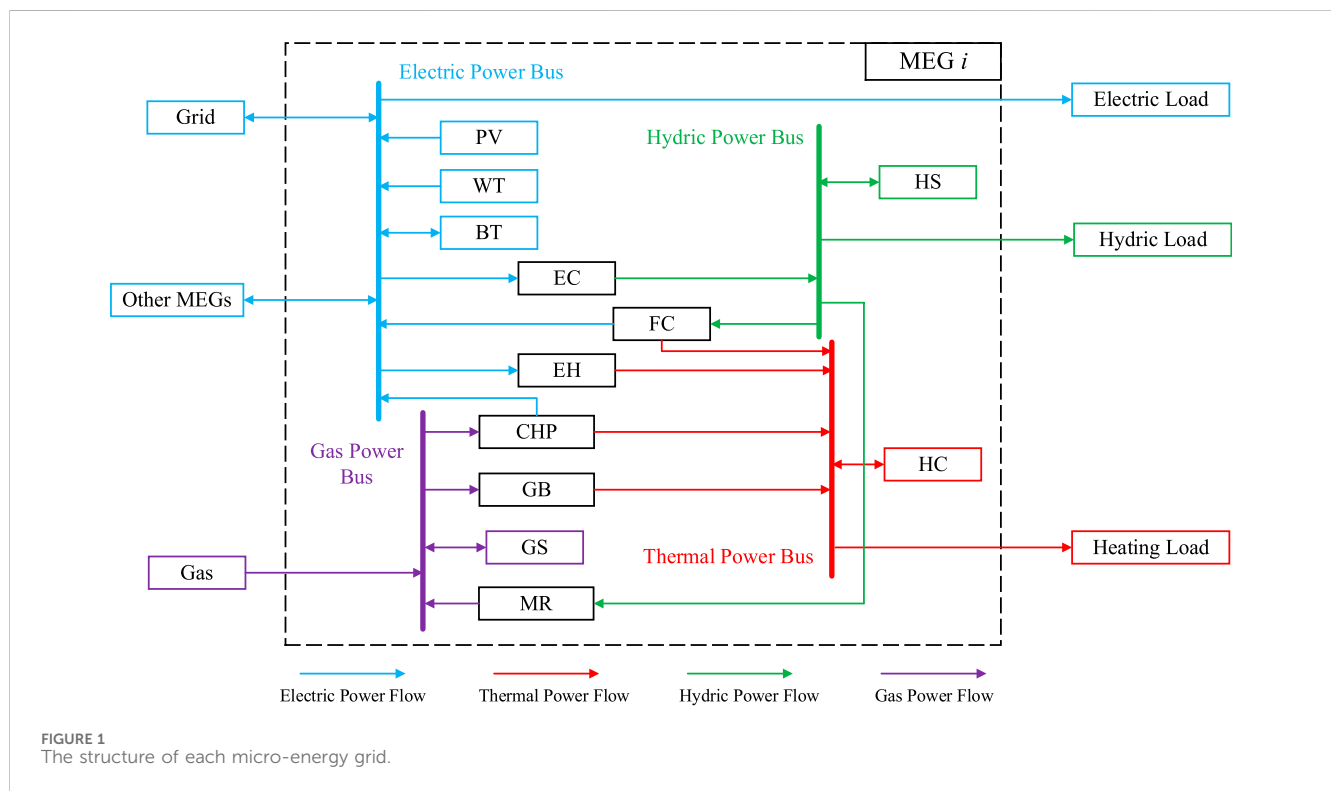
2.3 Comparison of main performance indicators of 3 P2H technologies

At present, there are three main types of electrolytic cells: alkaline electrolytic cells (AECs), proton exchange membrane electrolytic cells (PEMECs), and solid oxide electrolytic cells (SOECs).

Among the three P2H technologies, AECs boast the earliest research and development efforts, the most matured technology, and the lowest equipment cost. Nonetheless, they encounter challenges such as the difficulty in completely isolating hydrogen-

TABLE 1 The main technical indicators of the three electrolytic cells.

Parameters	AEC	PEMEC	SOEC
Current density (A/cm ²)	0.25–0.45	1.0–2.0	0.3–1.0
Voltage range (V)	1.87–2.10	1.65–1.85	1.78–1.85
Hydrogen production capacity (Nm ³ /h)	1,400	400	<10
Electricity consumption (kWh/Nm ³)	4.2–4.8	4.4–5.0	3.0
Operating temperature (°C)	50–100	80–100	120
Efficiency (%)	62–82	74–87	90–100
Startup time	1–5min	<10s	15min
Investment cost (Thousand RMB/kW)	2.2–10.5	9.8–14.7	>14
Efficiency attenuation (%/year)	0.25–0.45	0.5–2.5	3–50
Minimum input power (Rated power %)	20–25	5–10	0



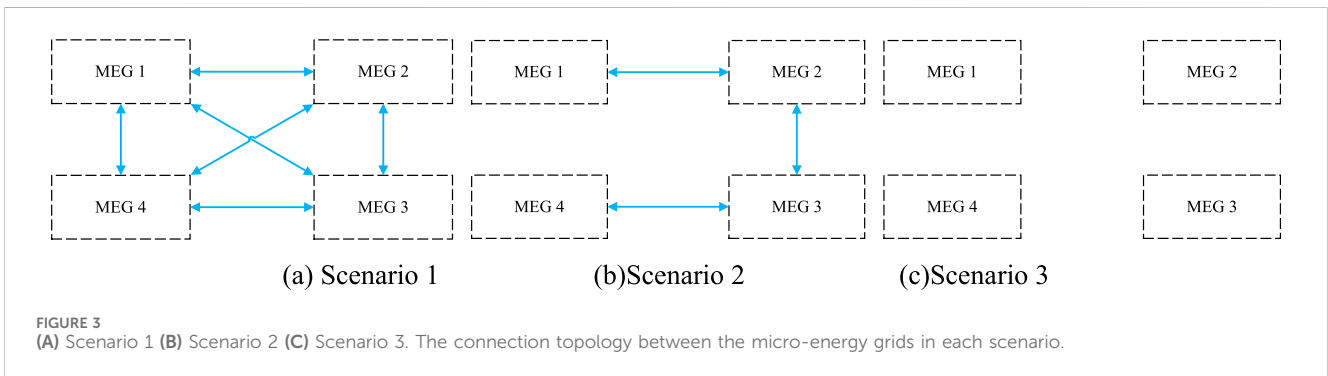
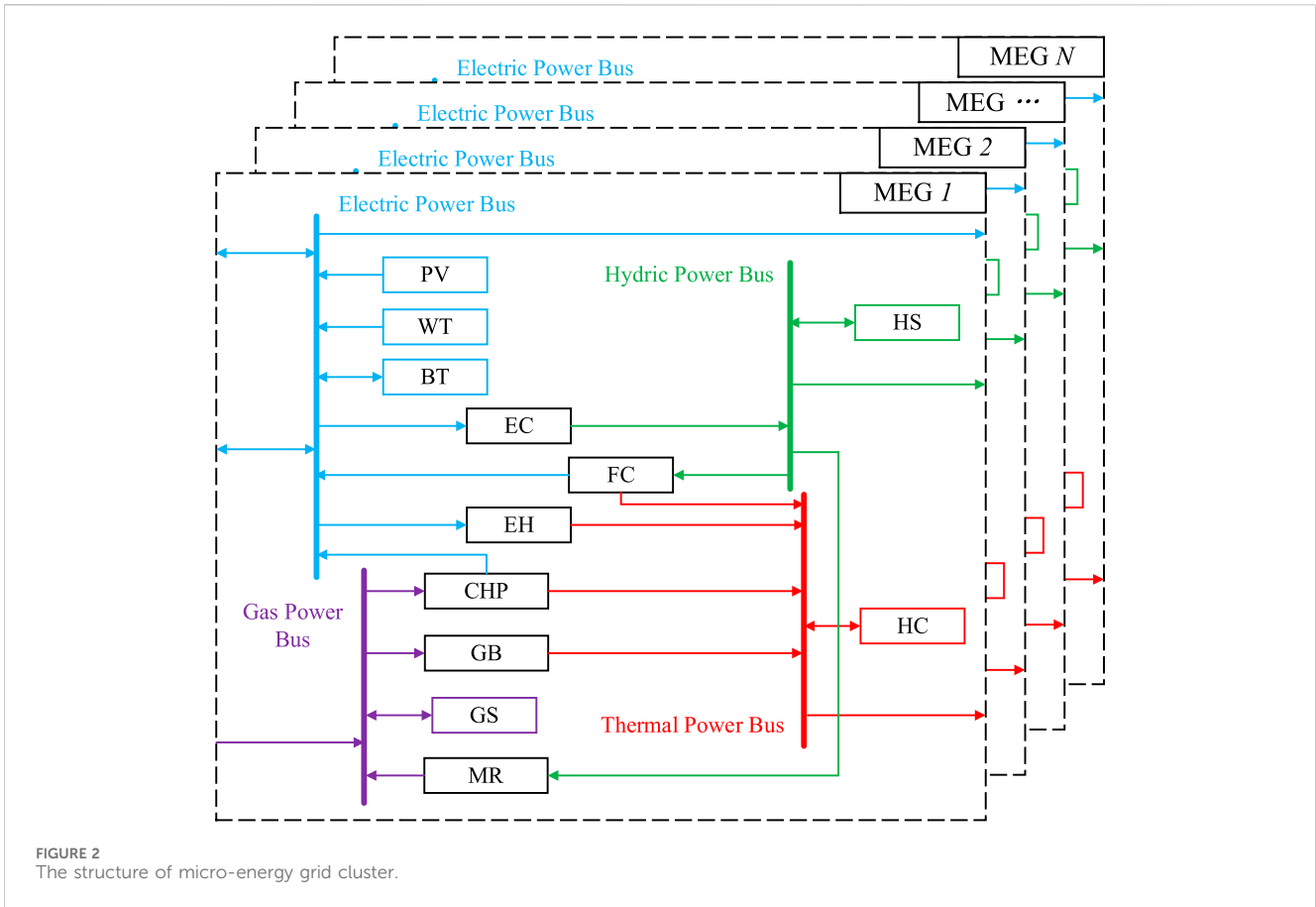
oxygen diffusion (especially under low loads), high electrolysis overvoltage, and the inertia of load ion conduction in electrolyte solutions. These factors limit their working load range and response speed.

In contrast, PEMECs have significantly improved load range and response speed compared to AECs, albeit with a slightly higher equipment cost. However, both AECs and PEMECs share a limitation: their rated hydrogen production efficiency does not exceed 70%.

SOECs, on the other hand, utilize solid oxide electrolytes to electrolyze gaseous water in high-temperature environments. By

harnessing the thermodynamics and kinetics of the electrolysis reaction, SOECs are able to improve energy conversion efficiency by approximately 10%–15%. However, due to the constraints of operating in high-temperature environments, SOEC technology currently lags behind PEMECs in terms of cost and response speed.

Table 1 below provides a concise overview of the key technical indicators associated with each of the three electrolytic cells. It is evident that each of the three P2H technologies offers distinct advantages: AEC excels in cost-efficiency, PEMEC stands out in terms of flexibility, while SOEC boasts the highest energy conversion efficiency.



3 Mathematical model for the optimal operation of micro-energy grids

3.1 System structure

The micro-energy grid incorporates a busbar design that comprises four essential power busbars: electricity, heat, hydrogen, and gas, as shown in Figure 1.

Within this micro-energy grid, the primary energy supply apparatus encompasses a harmonious blend of renewable energy generation systems and CHP units. Furthermore, the system is augmented by EH techniques and GB, enhancing the thermal

energy supply capabilities. Within this intricate system, devices such as EC and FC play pivotal roles, facilitating seamless interconversion between electrical and hydrogen energy. Notably, the hydrogen energy generation process inherently yields thermal energy, thus further augmenting the grid’s thermal output. Moreover, the refined hydrogen energy can undergo MR for conversion into natural gas, expanding the grid’s energy portfolio.

This versatile micro-energy grid caters to three primary load demands: electrical energy, hydrogen energy, and thermal energy, ensuring a comprehensive range of energy services. Its input energy sources are diverse, incorporating electricity sourced directly from the main power grid or exchanged with other micro-energy grids, as well as

TABLE 2 TOU electricity price.

Period	Time	Price/[RMB/(kWh)]
Valley	23:00–07:00	0.47
Off-peak	07:00–08:00, 11:00–18:00	0.87
Peak	08:00–11:00, 18:00–23:00	1.09

TABLE 3 Capacity of the devices installed in each micro-energy grid.

Devices	MEG 1	MEG 2	MEG 3	MEG 4
PV (kW)	1,000	1,000	1,000	3,000
WT (kW)	1,000	1,000	1,000	3,000
CHP (kW)	5,000	5,000	5,000	5,000
FC (kW)	1,000	1,000	3,000	1,000
EC (kW)	1,000	1,000	3,000	1,000
EH (kW)	2000	2000	2000	2000
GB (kW)	3,000	3,000	3,000	3,000
MR (kW)	1,000	1,000	1,000	1,000
BT (kWh)	1,000	1,000	1,000	1,000
HC (kWh)	1,000	1,000	1,000	1,000
HS (kWh)	1,000	1,000	1,000	1,000
GS (kWh)	1,000	1,000	1,000	1,000

natural gas procured efficiently from gas utility companies. This integrated approach fosters a resilient and sustainable energy ecosystem, tailored to meet the evolving needs of modern communities.

The article delves into an integrated energy system encompassing electric, thermal, and hydrogen components, which comprises a cluster of interconnected micro-energy grids, as depicted in Figure 2. These micro-energy grids are capable of exchanging electrical power seamlessly through dedicated interconnection lines, fostering a dynamic and interactive network.

3.2 Objective function

For each micro-energy grid, the overarching objective is to minimize operating costs, as outlined in Equation 4. These costs comprise four distinct components: operational and maintenance costs, gas procurement costs, electricity acquisition costs, and power exchange costs.

$$\min C^i = C_{OM}^i + C_{gas}^i + C_{grid}^i + C_{EX}^i \quad (4)$$

where C_{OM}^i represents operational and maintenance costs, C_{gas}^i represents gas procurement costs, C_{grid}^i represents electricity acquisition costs, C_{EX}^i represents power exchange costs.

The operational and maintenance costs are shown in Equations 5, 6.

$$C_{OM}^i = \sum_{t=1}^T \left(C_{PV,om}^{i,t} + C_{WT,om}^{i,t} + C_{CHP,om}^{i,t} + C_{FC,om}^{i,t} + C_{EC,om}^{i,t} + C_{EH,om}^{i,t} + C_{GB,om}^{i,t} + C_{MR,om}^{i,t} + C_{BT/HC/HS/GS,om}^{i,t} \right) \cdot \Delta t \quad (5)$$

$$C_{PV,om}^{i,t} = c_{PV,om}^{i,t} \cdot P_{PV,out}^{i,t}$$

$$C_{WT,om}^{i,t} = c_{WT,om}^{i,t} \cdot P_{WT,out}^{i,t}$$

$$C_{CHP,om}^{i,t} = c_{CHP,om}^{i,t} \cdot P_{CHP,out,E}^{i,t}$$

$$C_{FC,om}^{i,t} = \sum_{k=1}^K (c_{FC,om}^{i,k,t} \cdot P_{FC,out,E}^{i,k,t})$$

$$C_{EC,om}^{i,t} = \sum_{k=1}^K (c_{EC,om,1}^{i,k,t} \cdot P_{EC,out}^{i,k,t} + c_{EC,om,2}^{i,k,t} \cdot P_{EC,in,2}^{i,k,t})$$

$$C_{EH,om}^{i,t} = c_{EH,om}^{i,t} \cdot P_{EH,out}^{i,t}$$

$$C_{GB,om}^{i,t} = c_{GB,om}^{i,t} \cdot P_{GB,out}^{i,t}$$

$$C_{MR,om}^{i,t} = c_{MR,om}^{i,t} \cdot P_{MR,out}^{i,t}$$

$$C_{BT/HC/HS/GS,om}^{i,t} = c_{BT/HC/HS/GS,om}^{i,t} \cdot \left(P_{BT/HC/HS/GS,c}^{i,t} + P_{BT/HC/HS/GS,d}^{i,t} \right) \quad (6)$$

The gas procurement costs are illustrated in Equation 7.

$$C_{gas}^i = \sum_{t=1}^T \frac{R_{FU}^{i,t}}{H_{FU}^{i,t}} \cdot P_{gas,b}^{i,t} \cdot \Delta t \quad (7)$$

The electricity acquisition costs from the power grid are shown in Equation 8.

$$C_{grid}^i = \sum_{t=1}^T (c_{GD,b}^{i,t} \cdot P_{GD,b}^{i,t} - c_{GD,s}^{i,t} \cdot P_{GD,s}^{i,t}) \cdot \Delta t \quad (8)$$

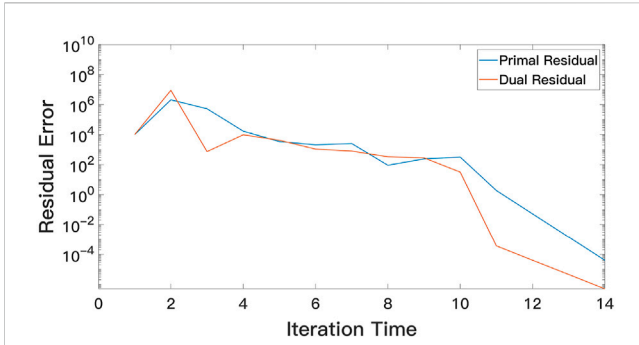


FIGURE 4 The variation of residual error with the iteration times in scenario 1

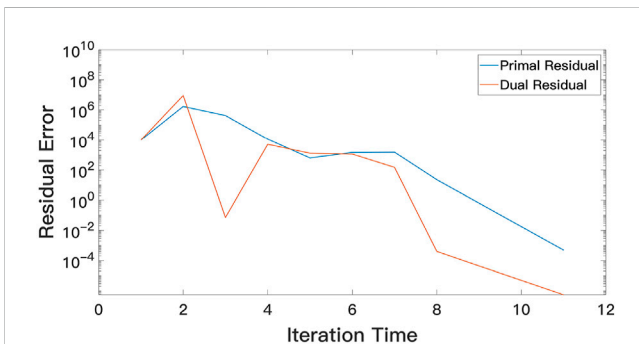


FIGURE 5 The variation of residual error with the iteration times in scenario 2.

The power exchange costs with other micro-energy grids are shown in Equation 9.

$$C_{EX}^i = \sum_{t=1}^T \sum_{j=1}^{IMG} c_{EX}^{i,j,t} \cdot (P_{EX,in}^{i,j,t} - P_{EX,out}^{i,j,t}) \cdot \Delta t \quad (9)$$

3.3 Constraints

3.3.1 Constraints on the power balance

The electric power balance is shown in Equation 10.

$$P_{BT,d,EX}^{i,t} + P_{GD,b}^{i,t} + P_{PV,out}^{i,t} + P_{WT,out}^{i,t} + P_{CHP,out,E}^{i,t} + \sum_{k=1}^K P_{FC,out,E}^{i,k,t} + \sum_{j=1}^{IMG} P_{EX,in}^{i,j,t} = P_{BT,c,EX}^{i,t} + P_{GD,s}^{i,t} + P_{EL}^{i,t} + \sum_{k=1}^K (P_{EC,in,1}^{i,k,t} + P_{EC,in,2}^{i,k,t}) + P_{EH,in}^{i,t} + \sum_{j=1}^{IMG} P_{EX,out}^{i,j,t} \quad (10)$$

The thermal power balance is shown in Equation 11.

$$P_{HC,d,EX}^{i,t} + P_{CHP,out,H}^{i,t} + P_{GB,out}^{i,t} + P_{EH,out}^{i,t} + \sum_{k=1}^K P_{FC,out,H}^{i,k,t} = P_{HC,c,EX}^{i,t} + P_{HL}^{i,t} \quad (11)$$

The hydric power balance is shown in Equation 12.

$$P_{HS,d,EX}^{i,t} + \sum_{k=1}^K P_{EC,out}^{i,k,t} = P_{HS,c,EX}^{i,t} + P_{HGL}^{i,t} + \sum_{k=1}^K P_{FC,in}^{i,k,t} + P_{MR,in}^{i,t} \quad (12)$$

The gas power balance is shown in Equation 13.

$$P_{GS,d,EX}^{i,t} + P_{gas,b}^{i,t} + P_{MR,out}^{i,t} = P_{GS,c,EX}^{i,t} + P_{CHP,in}^{i,t} + P_{GB,in}^{i,t} \quad (13)$$

3.3.2 Constraints on the purchased power of electricity and gas

The purchased/sold electric power constraints from/to the power grid are shown in Equation 14.

$$\begin{aligned} x_{GD,b}^{i,t} \cdot P_{GD,b,\min}^{i,t} &\leq P_{GD,b}^{i,t} \leq x_{GD,b}^{i,t} \cdot P_{GD,b,\max}^{i,t} \\ x_{GD,s}^{i,t} \cdot P_{GD,s,\min}^{i,t} &\leq P_{GD,s}^{i,t} \leq x_{GD,s}^{i,t} \cdot P_{GD,s,\max}^{i,t} \\ 0 &\leq x_{GD,b}^{i,t} + x_{GD,s}^{i,t} \leq 1 \end{aligned} \quad (14)$$

The purchased gas power constraints from the gas company are shown in Equation 15.

$$P_{gas,b,\min}^{i,t} \leq P_{gas,b}^{i,t} \leq P_{gas,b,\max}^{i,t} \quad (15)$$

3.3.3 Constraints on the efficiency of the devices

The efficiency constraints of the devices are shown in Equation 16.

$$\begin{aligned} P_{CHP,out,E}^{i,t} &= \eta_{CHP,E}^{i,t} \cdot P_{CHP,in}^{i,t} \\ P_{CHP,out,H}^{i,t} &= V_{CHP}^{i,t} \cdot P_{CHP,out,E}^{i,t} \\ P_{FC,out,E}^{i,k,t} &= \eta_{FC,E}^{i,k,t} \cdot P_{FC,in}^{i,k,t} \\ P_{FC,out,H}^{i,k,t} &= V_{FC}^{i,k,t} \cdot P_{FC,out,E}^{i,k,t} \\ P_{EC,out}^{i,k,t} &= \eta_{EC}^{i,k,t} \cdot P_{EC,in,1}^{i,k,t} \\ P_{EH,out}^{i,t} &= \eta_{EH}^{i,t} \cdot P_{EH,in}^{i,t} \\ P_{GB,out}^{i,t} &= \eta_{GB}^{i,t} \cdot P_{GB,in}^{i,t} \\ P_{MR,out}^{i,t} &= \eta_{MR}^{i,t} \cdot P_{MR,in}^{i,t} \end{aligned} \quad (16)$$

3.3.4 Constraints on the upper and lower power limits of the devices

The upper and lower power limit constraints are shown in Equation 17.

$$\begin{aligned} 0 &\leq P_{PV,out}^{i,t} \leq \delta_{PV,fore}^{i,t} \cdot Cap_{PV}^i \\ 0 &\leq P_{WT,out}^{i,t} \leq \delta_{WT,fore}^{i,t} \cdot Cap_{WT}^i \\ \delta_{CHP,out,E,\min}^{i,t} \cdot Cap_{CHP,E}^i &\leq P_{CHP,out,E}^{i,t} \leq \delta_{CHP,out,E,\max}^{i,t} \cdot Cap_{CHP,E}^i \\ \delta_{FC,out,E,\min}^{i,k,t} \cdot Cap_{FC,E}^{i,k} &\leq P_{FC,out,E}^{i,k,t} \leq \delta_{FC,out,E,\max}^{i,k,t} \cdot Cap_{FC,E}^{i,k} \\ x_{EC}^{i,k,t} \cdot \delta_{EC,out,\min}^{i,k,t} \cdot Cap_{EC}^i &\leq P_{EC,out}^{i,k,t} \leq x_{EC}^{i,k,t} \cdot \delta_{EC,out,\max}^{i,k,t} \cdot Cap_{EC}^i \\ \delta_{EH,out,\min}^{i,t} \cdot Cap_{EH}^i &\leq P_{EH,out}^{i,t} \leq \delta_{EH,out,\max}^{i,t} \cdot Cap_{EH}^i \\ \delta_{GB,out,\min}^{i,t} \cdot Cap_{GB}^i &\leq P_{GB,out}^{i,t} \leq \delta_{GB,out,\max}^{i,t} \cdot Cap_{GB}^i \\ \delta_{MR,out,\min}^{i,t} \cdot Cap_{MR}^i &\leq P_{MR,out}^{i,t} \leq \delta_{MR,out,\max}^{i,t} \cdot Cap_{MR}^i \end{aligned} \quad (17)$$

3.3.5 Constraints on the ramping limit

The ramping limit constraints are shown in Equation 18.

$$\begin{aligned} P_{CHP,out,E}^{i,t} - P_{CHP,out,E}^{i,t-1} &\leq \delta_{CHP,ramp,\max}^i \cdot Cap_{CHP,E}^i \\ P_{FC,out,E}^{i,k,t} - P_{FC,out,E}^{i,k,t-1} &\leq \delta_{FC,ramp,\max}^{i,k} \cdot Cap_{FC,E}^{i,k} \\ P_{EC,out}^{i,k,t} - P_{EC,out}^{i,k,t-1} &\leq \delta_{EC,ramp,\max}^{i,k} \cdot Cap_{EC}^{i,k} \end{aligned} \quad (18)$$

TABLE 4 Comparison of the optimization results between ADMM algorithm and centralized optimization method.

Total cost	Scenario 1	Scenario 2	Scenario 3
ADMM (× 10 ⁴ RMB)	1229.2547	1447.0512	1821.1192
Centralized Optimization (× 10 ⁴ RMB)	1225.0296	1434.3320	1820.5015
Percentage error	0.3449%	0.8868%	0.0339%

TABLE 5 The costs of each part of each micro-energy grid in scenario 1 (× 10⁴ RMB).

	Total	C _{OM}	C _{gas}	C _{grid}	C _{EX}
MEG 1	278.3116	46.3552	291.7262	-61.1824	1.4184
MEG 2	1,213.0038	83.1731	782.3969	-43.0653	390.5047
MEG 3	227.5857	45.2098	182.7660	-49.4083	49.0237
MEG 4	-489.6465	75.3573	78.9783	-203.0170	-440.9614
Total	1229.2547	250.0955	1335.8674	-356.6730	-0.0146

TABLE 6 The costs of each part of each micro-energy grid in scenario 2 (× 10⁴ RMB).

	Total	C _{OM}	C _{gas}	C _{grid}	C _{EX}
MEG 1	368.6905	48.2351	453.8950	-38.5750	-94.8646
MEG 2	1347.4063	84.1113	850.4238	116.3950	296.4769
MEG 3	246.0414	44.5781	200.0632	-116.3188	117.7186
MEG 4	-515.0870	72.5835	4.0948	-272.4343	-319.3309
Total	1447.0512	249.5080	1508.4768	-310.9332	0.0001

3.3.6 Constraints on the energy storage devices

The limitations pertaining to the energy storage device are delineated in Equations 19–21. Specifically, Equation 19 encapsulates the efficiency constraint during charging and discharging operations, Equation 20 outlines the upper and lower bounds for the charging and discharging power, and Equation 21 specifies the energy capacity constraint of the storage device.

$$\begin{aligned}
 P_{BT/HC/HS/GS,c}^{i,t} &= \eta_{BT/HC/HS/GS,c}^{i,t} P_{BT/HC/HS/GS,c,EX}^{i,t} \\
 P_{BT/HC/HS/GS,d,EX}^{i,t} &= \eta_{BT/HC/HS/GS,d}^{i,t} P_{BT/HC/HS/GS,d}^{i,t}
 \end{aligned}
 \tag{19}$$

$$\begin{aligned}
 x_{BT/HC/HS/GS,c}^{i,t} \cdot \delta_{BT/HC/HS/GS,c,\min}^{i,t} \cdot Cap_{BT/HC/HS/GS,c}^i &\leq P_{BT/HC/HS/GS,c}^{i,t} \\
 P_{BT/HC/HS/GS,c}^{i,t} &\leq x_{BT/HC/HS/GS,c}^{i,t} \cdot \delta_{BT/HC/HS/GS,c,\max}^{i,t} \cdot Cap_{BT/HC/HS/GS,c}^i \\
 x_{BT/HC/HS/GS,d}^{i,t} \cdot \delta_{BT/HC/HS/GS,d,\min}^{i,t} \cdot Cap_{BT/HC/HS/GS,d}^i &\leq P_{BT/HC/HS/GS,d}^{i,t} \\
 P_{BT/HC/HS/GS,d}^{i,t} &\leq x_{BT/HC/HS/GS,d}^{i,t} \cdot \delta_{BT/HC/HS/GS,d,\max}^{i,t} \cdot Cap_{BT/HC/HS/GS,d}^i \\
 0 \leq x_{BT/HC/HS/GS,c}^{i,t} + x_{BT/HC/HS/GS,d}^{i,t} &\leq 1
 \end{aligned}
 \tag{20}$$

$$\begin{aligned}
 v_{BT/HC/HS/GS,\min}^{i,t} \cdot Cap_{BT/HC/HS/GS}^i W_{BT/HC/HS/GS}^{i,t+1} &\leq W_{BT/HC/HS/GS}^{i,t} \leq v_{BT/HC/HS/GS,\max}^{i,t} \\
 &\cdot Cap_{BT/HC/HS/GS}^i W_{BT/HC/HS/GS}^{i,t+1} \\
 &= W_{BT/HC/HS/GS}^{i,t} \left(1 - \sigma_{BT/HC/HS/GS}^i \right) \\
 &+ \left(P_{BT/HC/HS/GS,c}^{i,t} - P_{BT/HC/HS/GS,d}^{i,t} \right) \\
 &\cdot \Delta t, (t = 0, \dots, T - 1) W_{BT/HC/HS/GS}^{i,T} \\
 &= W_{BT/HC/HS/GS}^{i,0}
 \end{aligned}
 \tag{21}$$

3.3.7 Constraints on the operation of the EC

As outlined in Section 3.2, the EC's upper and lower power constraints, initial power constraints, and start-stop state limitations are defined in Equations 22, 23. Furthermore, Equation 24 stipulates that the start-stop state must remain consistent at the beginning and end of each cycle, while Equation 25 imposes a maximum limit on the number of starts and stops that can occur within a single cycle.

$$\begin{aligned}
 x_{EC}^{i,k,t} \cdot \delta_{EC,in,1,\min}^{i,k} \cdot Cap_{EC}^{i,k} &\leq P_{EC,in,1}^{i,k,t} \leq x_{EC}^{i,k,t} \cdot \delta_{EC,in,1,\max}^{i,k} \cdot Cap_{EC}^{i,k} \\
 P_{EC,in,2}^{i,k,t} &= \sum_{\tau=0}^{\alpha_{EC}-1} y_{EC}^{i,k,t-\tau} \cdot \delta_{EC,boot}^{i,k} \cdot Cap_{EC}^{i,k}
 \end{aligned}
 \tag{22}$$

$$\begin{aligned}
 y_{EC}^{i,k,t-\alpha_{EC}} - z_{EC}^{i,k,t} &= x_{EC}^{i,k,t} - x_{EC}^{i,k,t-1} \\
 y_{EC}^{i,k,t} &\leq 1 - x_{EC}^{i,k,t-1} \\
 z_{EC}^{i,k,t} &\leq x_{EC}^{i,k,t-1}
 \end{aligned}
 \tag{23}$$

$$x_{EC}^{i,k,T} = x_{EC}^{i,k,0}
 \tag{24}$$

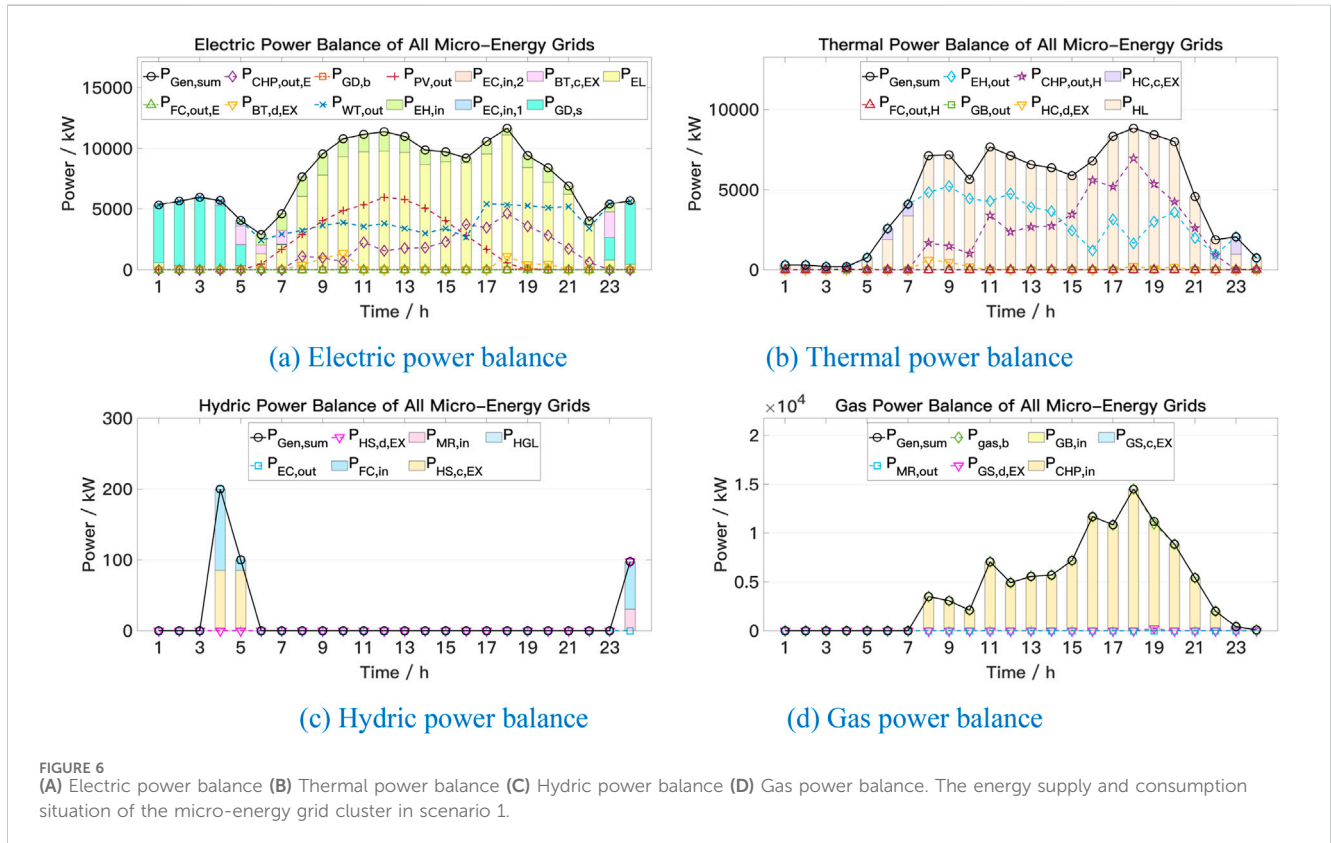
$$\begin{aligned}
 \sum_{t=1}^T y_{EC}^{i,k,t} &\leq y_{EC,\max}^{i,k} \\
 \sum_{t=1}^T z_{EC}^{i,k,t} &\leq z_{EC,\max}^{i,k}
 \end{aligned}
 \tag{25}$$

3.3.8 Constraints on the exchanged power with other micro-energy grids

Equation 26 establishes the upper and lower bounds for the interactive power exchange with other micro-energy grids. Meanwhile, Equation 27 stipulates that the diagonal elements of the

TABLE 7 The costs of each part of each micro-energy grid in scenario 3 ($\times 10^4$ RMB).

	Total	C_{OM}	C_{gas}	C_{grid}	C_{EX}
MEG 1	295.2441	47.3659	321.8564	-73.9782	0
MEG 2	1730.3632	88.7430	974.1874	667.4329	0
MEG 3	267.9580	47.1172	267.4596	-46.6189	0
MEG 4	-472.4460	69.8329	0.9230	-543.2019	0
Total	1821.1192	253.0590	1564.4263	3.6339	0



interaction state matrix must be zero, indicating that a grid cannot interact with itself, and furthermore, there can be no more than one input and one output state that is assigned a value of 1, signifying a single connection for power exchange in either direction.

$$A_{EX}^{i,j,t} \cdot x_{EX,out}^{i,j,t} \cdot P_{EX,min}^{i,j,t} \leq P_{EX,out}^{i,j,t} \leq A_{EX}^{i,j,t} \cdot x_{EX,out}^{i,j,t} \cdot P_{EX,max}^{i,j,t} \quad (26)$$

$$A_{EX}^{i,j,t} \cdot x_{EX,in}^{i,j,t} \cdot P_{EX,min}^{i,j,t} \leq P_{EX,in}^{i,j,t} \leq A_{EX}^{i,j,t} \cdot x_{EX,in}^{i,j,t} \cdot P_{EX,max}^{i,j,t} \quad (27)$$

$$x_{EX,out}^{i,i,t} \cdot x_{EX,in}^{i,i,t} = 0$$

$$x_{EX,out}^{i,j,t} + x_{EX,in}^{i,j,t} \leq 1$$

4 Algorithm for solving the multi-agent collaborative optimization model

4.1 ADMM algorithm

As a distributed algorithm, ADMM excels in addressing large-scale separable optimization problems by systematically

breaking them down into smaller subproblems. This strategic decomposition not only simplifies the complexity but also paves the way for the precise identification of the elusive global optimal solution. The method seamlessly integrates the decomposition principles of the dual ascent method with the superior convergence properties of the Lagrange multiplier method, creating a potent synergy that ensures both robustness and unparalleled effectiveness.

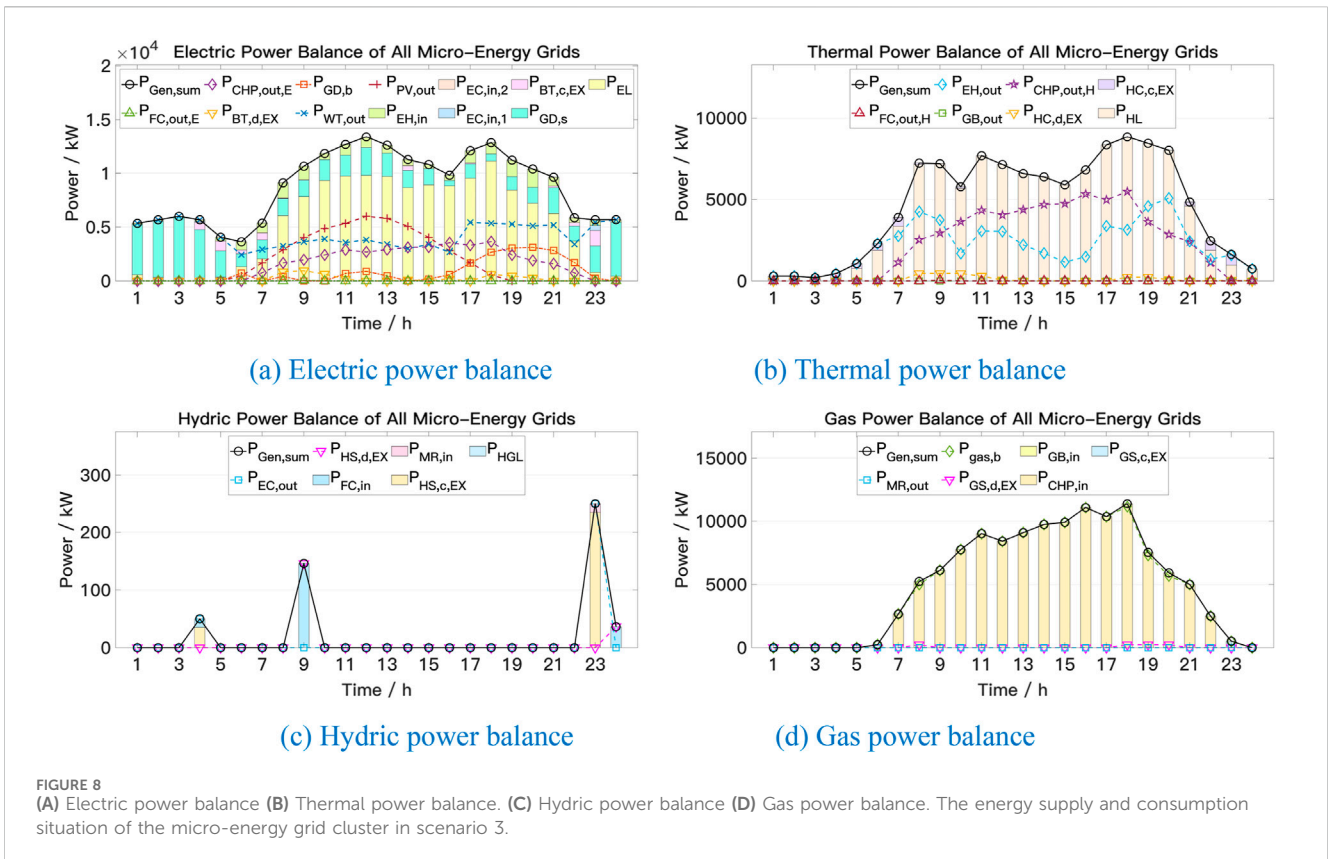
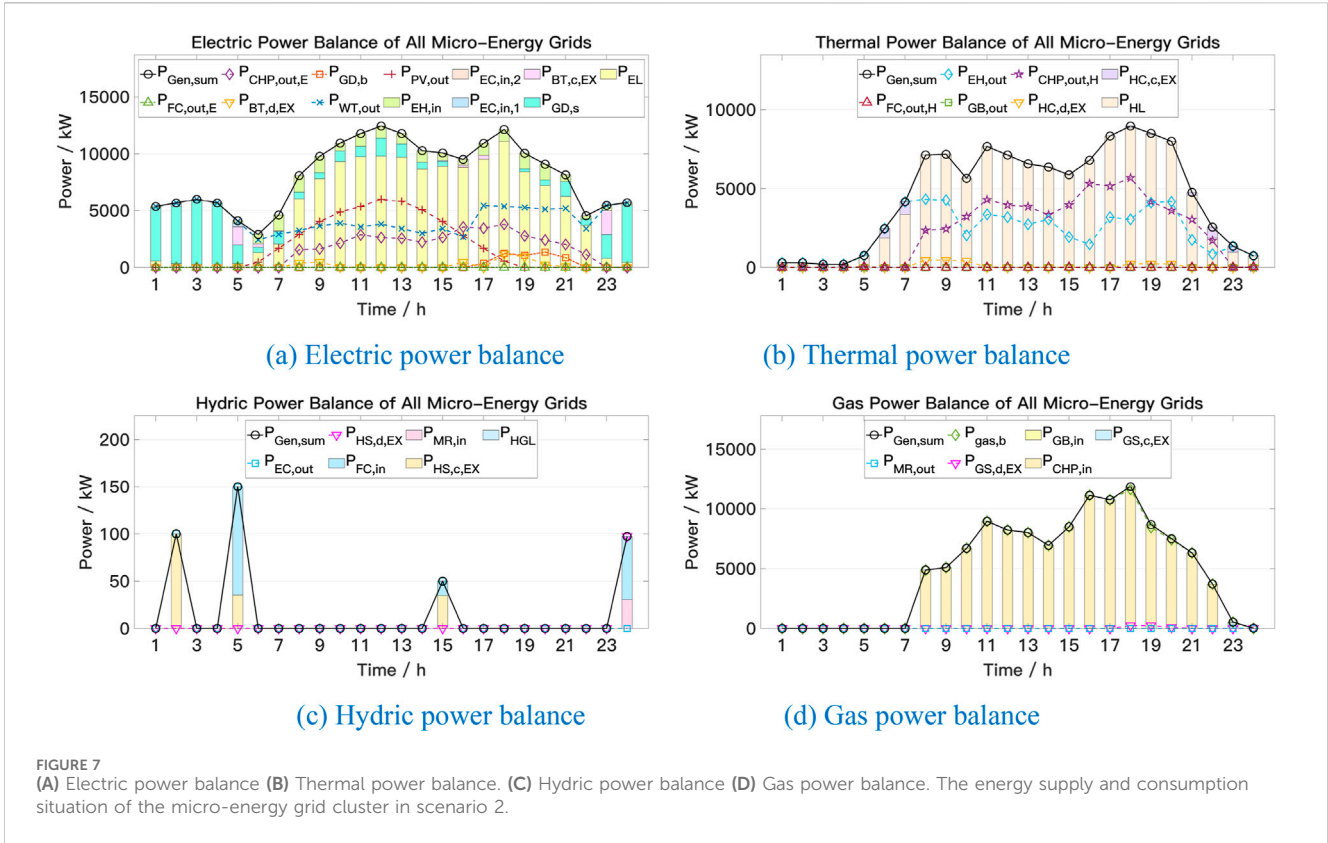
The process of solving the problem shown in Equation 28 using the ADMM algorithm is as follows.

$$\min_x f(x) \quad (28)$$

$$s.t. Ax = b$$

where $x \in \mathbb{R}^u$ is the decision variable, $f(\cdot)$ is the objective function, $A \in \mathbb{R}^{p \times u}$ is the coefficient matrix, and $b \in \mathbb{R}^p$ is the coefficient vector.

Split decision variable x in Equation 28 into two decision variables y and z , as delineated in Equation 29:



$$\begin{aligned} \min_{y,z} & g(y) + h(z) \\ \text{s.t.} & Cy + Dz = e \end{aligned} \quad (29)$$

where $y \in \mathbb{R}^n$ and $z \in \mathbb{R}^m$ are decision variables, $g(\cdot)$ and $h(\cdot)$ are sub optimization objectives, $C \in \mathbb{R}^{p \times n}$ and $D \in \mathbb{R}^{p \times m}$ are coefficient matrices, and $e \in \mathbb{R}^p$ is coefficient vector.

By incorporating a quadratic penalty term into the Lagrangian function, an augmented Lagrangian function is derived, providing an enhanced framework for addressing optimization problems, which is shown in Equation 30:

$$L_\rho(y, z, \lambda) = g(y) + h(z) + \lambda^T(Cy + Dz - e) + \frac{\rho}{2} \|Cy + Dz - e\|_2^2 \quad (30)$$

where $\lambda \in \mathbb{R}^p$ is the Lagrange multiplier, and $\rho > 0$ is the penalty factor.

Alternately solve variables y and z , and update the Lagrange multiplier, as shown in Equation 31, until the convergence condition is met.

$$\begin{cases} y^{m+1} = \operatorname{argmin}_y L_\rho(y, z^m, \lambda^m) \\ z^{m+1} = \operatorname{argmin}_z L_\rho(y^{m+1}, z, \lambda^m) \\ \lambda^{m+1} = \lambda^m + \rho(Cy^{m+1} + Dz^{m+1} - e) \end{cases} \quad (31)$$

where m stands for iterations.

4.2 Multi agent optimal operation model based on ADMM algorithm

Utilizing the mathematical model outlined in Chapter 3 for the optimal operation of micro-energy grids, and leveraging the power of the ADMM algorithm, the objective function is restructured in the following manner, as illustrated in Equation 32:

$$\min C^i = C_{OM}^i + C_{gas}^i + C_{grid}^i + C_{EX}^i + C_{Lag}^i + C_{Pen}^i \quad (32)$$

where C_{Lag}^i represents the Lagrange multiplier term, and C_{Pen}^i is the penalty term, which are illustrated in Equations 33, 34.

$$C_{Lag}^i = \sum_{j=1}^{IMG} \sum_{t=1}^T \lambda_{EX,out}^{i,j,t,m} \cdot (P_{EX,out}^{i,j,t} - P_{EX,out,ref}^{i,j,t,m}) + \sum_{j=1}^{IMG} \sum_{t=1}^T \lambda_{EX,in}^{i,j,t,m} \cdot (P_{EX,in}^{i,j,t} - P_{EX,in,ref}^{i,j,t,m}) \quad (33)$$

$$C_{Pen}^i = \frac{1}{2} \rho_{EX,out}^{i,m} \sum_{j=1}^{IMG} \sum_{t=1}^T (P_{EX,out}^{i,j,t} - P_{EX,out,ref}^{i,j,t,m})^2 + \frac{1}{2} \rho_{EX,in}^{i,m} \times \sum_{j=1}^{IMG} \sum_{t=1}^T (P_{EX,in}^{i,j,t} - P_{EX,in,ref}^{i,j,t,m})^2 \quad (34)$$

The constraints specified in Equation 10 through Equation 27 maintain their original form and remain unaltered.

4.3 The solving process

The process of employing the ADMM algorithm to address this problem is outlined below:

1. Start with $m = 1$. Set the convergence thresholds $\epsilon_{EX,pri}$ and $\epsilon_{EX,dual}$ for the primal and dual residuals. Initialize the dual multipliers $\lambda_{EX,out}^{i,j,t,1}$ and $\lambda_{EX,in}^{i,j,t,1}$, penalty factors $\rho_{EX,out}^{i,1}$ and $\rho_{EX,in}^{i,1}$, and coordinate variables $P_{EX,out,ref}^{i,j,t,1}$ and $P_{EX,in,ref}^{i,j,t,1}$.
2. Solve each subproblem individually.
3. Update the coordination variables $P_{EX,out,ref}^{i,j,t,m+1}$ and $P_{EX,in,ref}^{i,j,t,m+1}$ as shown in Equation 35.

$$\begin{aligned} P_{EX,out,ref}^{i,j,t,m+1} &= \frac{1}{2} (P_{EX,out}^{i,j,t} + P_{EX,in}^{j,i,t}) \\ P_{EX,in,ref}^{i,j,t,m+1} &= \frac{1}{2} (P_{EX,in}^{i,j,t} + P_{EX,out}^{j,i,t}) \end{aligned} \quad (35)$$

4. Compute the primal residual $r_{EX,pri}^{m+1}$ and the dual residual $r_{EX,dual}^{m+1}$, which are encapsulated in Equation 36, and assess their convergence based on conditions Equation 37.

$$\begin{aligned} r_{EX,pri}^{m+1} &= \sum_{i=1}^{IMG} \sum_{j=1}^{IMG} \sum_{t=1}^T (P_{EX,out}^{i,j,t} - P_{EX,out,ref}^{i,j,t,m})^2 + \sum_{i=1}^{IMG} \times \sum_{j=1}^{IMG} \sum_{t=1}^T (P_{EX,in}^{i,j,t} - P_{EX,in,ref}^{i,j,t,m})^2 r_{EX,dual}^{m+1} \\ &= \sum_{i=1}^{IMG} \sum_{j=1}^{IMG} \sum_{t=1}^T (P_{EX,out,ref}^{i,j,t,m+1} - P_{EX,out,ref}^{i,j,t,m})^2 + \sum_{i=1}^{IMG} \times \sum_{j=1}^{IMG} \sum_{t=1}^T (P_{EX,in,ref}^{i,j,t,m+1} - P_{EX,in,ref}^{i,j,t,m})^2 \end{aligned} \quad (36)$$

$$\begin{aligned} r_{EX,pri}^{m+1} &\leq \epsilon_{EX,pri} \\ r_{EX,dual}^{m+1} &\leq \epsilon_{EX,dual} \end{aligned} \quad (37)$$

5. Adjust the penalty factors $\rho_{EX,out}^{i,m+1}$ and $\rho_{EX,in}^{i,m+1}$ as expressed in Equation 38.

$$\rho_{EX,out/in}^{i,m+1} = \begin{cases} \omega_{EX,i} \cdot \rho_{EX,out/in}^{i,m} r_{EX,pri}^{m+1} \geq \chi_{EX} s_{EX,dual}^{m+1} \\ \omega_{EX,d} \cdot \rho_{EX,out/in}^{i,m} s_{EX,dual}^{m+1} \geq \chi_{EX} r_{EX,pri}^{m+1} \\ \rho_{EX,out/in}^{i,m} \text{ else} \end{cases} \quad (38)$$

6. Update the dual multipliers $\lambda_{EX,out}^{i,j,t,m+1}$ and $\lambda_{EX,in}^{i,j,t,m+1}$, and increment m by 1 ($m = m + 1$), which are defined in Equation 39.

$$\begin{aligned} \lambda_{EX,out}^{i,j,t,m+1} &= \lambda_{EX,out}^{i,j,t,m} + \rho_{EX,out}^{i,m} \cdot (P_{EX,out}^{i,j,t} - P_{EX,out,ref}^{i,j,t,m}) \\ \lambda_{EX,in}^{i,j,t,m+1} &= \lambda_{EX,in}^{i,j,t,m} + \rho_{EX,in}^{i,m} \cdot (P_{EX,in}^{i,j,t} - P_{EX,in,ref}^{i,j,t,m}) \end{aligned} \quad (39)$$

Repeat steps 2 through 6 until the desired convergence criteria are met.

5 Case studies

5.1 Description of the scenarios

In the case studies, three distinct operational scenarios were delineated: fully connected, partially connected, and independent operation, as depicted in Figure 3. The objective was to delve into the implications of varying connection topologies on the operational efficiency of micro-energy grid clusters. Specifically, in each of these scenarios, micro-energy grid 2 experienced a higher load level,

micro-energy grid 3 boasted a larger capacity for hydrogen production devices, and micro-energy grid 4 generated a more significant amount of renewable energy.

The cost of procuring electricity from the power grid is determined by the time-of-use pricing model, as outlined in Table 2. Meanwhile, Table 3 provides a comprehensive overview of the installed devices capacity within each micro-energy grid.

5.2 Convergence analysis

The convergence curves for the ADMM under Scenario 1 and Scenario 2 are presented in Figures 4, 5 respectively. As evident from the graphs, after exceeding ten iterations, the algorithm successfully converges to the designated threshold.

Furthermore, in Scenario 3, where the 4 micro-energy grids operate independently, the exchanged power between them inevitably amounts to 0. Consequently, the ADMM algorithm achieves convergence after the initial iteration.

5.3 Economic analysis

Table 4 presents a comparative analysis of the total costs incurred by the ADMM algorithm and the centralized optimization method across three distinct scenarios. Notably, it is evident that in each of these scenarios, the ADMM algorithm's error margin remains consistently below 1%, thus conclusively affirming the robustness and effectiveness of the proposed algorithm.

Tables 5–7 illustrate the breakdown of costs for each component of the micro-energy grids across three distinct scenarios. A noteworthy trend emerges, indicating that as the connection topology weakens, the total cost of micro-energy grid clusters rises incrementally. This underscores the pivotal role of power interchange between micro-energy grids in minimizing overall costs. Notably, micro-energy grid 2, which bears a heavier load, exhibits the most significant cost variation. The interaction of power between micro-energy grids substantially mitigates their electricity and gas procurement costs. Furthermore, despite micro-energy grid 1 and micro-energy grid 3 having comparable load levels, their costs differ due to the presence of electric hydrogen production equipment in the latter, which facilitates the storage of a portion of electrical energy.

5.4 Operation analysis

Figures 6–8 illustrate the operational dynamics of micro-energy grid clusters across three distinct scenarios. Notably, apart from renewable energy generation, CHP emerges as the primary source of electricity, while CHP and EH jointly constitute the main supply methods for thermal energy. As the interconnection topology between micro-energy grids weakens, a noteworthy surge in the output of CHP and grid-purchased power is observed. This increase arises from the inability to transmit excess electricity to other micro-energy grids via connecting lines, leading to its sale to the grid. Consequentially, this trend also prompts an augmentation in

gas purchasing power. Additionally, energy storage devices play a pivotal role in effectively managing peak and valley load conditions, enabling effective load shaving and valley filling.

6 Conclusion

This article delves into the distributed optimization operation method for micro-energy grid clusters, focusing on the integrated energy system encompassing electricity, heat, and hydrogen. In developing the mathematical model for the electrolytic cell, we accounted for its startup characteristics to ensure an accurate portrayal of the P2H conversion process. With regard to optimizing the model algorithms, we established an optimization operation model centered on each micro-energy grid, taking into consideration their respective interests and demands. For distributed solution, we employed the ADMM algorithm. A case analysis revealed that the variance in total operating costs, attributed to different connection topologies between micro-energy grids, could be as significant as 48.15%. Furthermore, a comparison with the results obtained from centralized optimization algorithms underscores the efficacy of the ADMM algorithm.

Data availability statement

The original contributions presented in the study are included in the article/supplementary material, further inquiries can be directed to the corresponding author.

Author contributions

DZ: Conceptualization, Data curation, Formal Analysis, Funding acquisition, Investigation, Methodology, Project administration, Resources, Software, Supervision, Validation, Visualization, Writing–original draft. JX: Data curation, Formal Analysis, Funding acquisition, Investigation, Methodology, Resources, Software, Writing–original draft. CZ: Data curation, Investigation, Methodology, Writing–original draft. PW: Data curation, Formal Analysis, Methodology, Software, Writing–original draft. GP: Methodology, Supervision, Writing–original draft. ZG: Methodology, Supervision, Writing–original draft.

Funding

The author(s) declare that financial support was received for the research, authorship, and/or publication of this article. The study was supported by “Science and Technology Project of State Grid Jiangsu Electric Power Co., Ltd. (Grant No. J2023072)”.

Conflict of interest

Authors DZ, JX, CZ, and PW were employed by State Grid Nanjing Power Supply Company.

The remaining authors declare that the research was conducted in the absence of any commercial or financial relationships that could be construed as a potential conflict of interest.

The authors declare that this study received funding from State Grid Jiangsu Electric Power Co., Ltd. The funder had the following involvement in the study: study design, data collection and analysis, writing of this article and decision to publish.

References

- Cao, W., Zhai, D., Zhang, J., Sha, H., Wang, Z., and Han, Q. (2022). "Study on optimal configuration of hydrogen energy storage IES with dual-fuel cells," in 2022 4th international conference on electrical engineering and control technologies (CEEECT), Shanghai, China, 16–18 December 2022 (IEEE), 939–946. doi:10.1109/CEEECT55960.2022.10030112
- Chen, Q., Xia, M., Chen, M., and Hu, H. (2018). *Distributed energy management for integrated energy system considering multiple independent operators*. Portland, OR, USA: IEEE Power & Energy Society General Meeting PESGM, 1–5. doi:10.1109/PESGM.2018.8586052
- Dong, Y., Ma, Z., Wang, Q., Ma, S., and Han, Z. (2023). "Optimal planning of multi-electrolyzer power-to-hydrogen (P2H) clusters in distribution network," in 2023 IEEE international conference on applied superconductivity and electromagnetic devices (ASEMD). Tianjin, China, October, 2023 (IEEE), 1–2. doi:10.1109/ASEMD59061.2023.10368814
- Gu, Z., Pan, G., Gu, W., Qiu, H., and Lu, S. (2024). Robust optimization of scale and revenue for integrated power-to-hydrogen systems within energy, ancillary services, and hydrogen markets. *IEEE Trans. Power Syst.* 39 (3), 5008–5023. doi:10.1109/TPWRS.2023.3323660
- Gu, Z., Pan, G., Gu, W., Zhou, S., Wu, Z., and Lu, S. (2023). Assessment and prospect of region joint electrolytic hydrogen systems considering multiple energy sources: wind, solar, hydro and thermal power. *IEEE Trans. Industry Appl.* 59 (5), 5269–5282. doi:10.1109/TIA.2023.3282923
- Gupta, M., Das, K., Friis-Møller, M., and Leon, J. P. M. (2023). "Assessment of hybrid power plant operation including P2H in future energy markets," in 22nd wind and solar integration workshop (WIW 2023). Copenhagen, Denmark, 289–294. doi:10.1049/icp.2023.2750
- He, X., Lu, T., Li, Y., Wang, S., and Li, J. (2021). Collaborative planning of integrated energy system considering P2H technology. *IEEE/IAS Industrial Commer. Power Syst. Asia (I&CPS Asia)*, 1219–1222. doi:10.1109/ICPSAsia52756.2021.9621567
- Huang, H., Li, Z., Sampath, L. P. M. I., Yang, J., Nguyen, H. D., Gooi, H. B., et al. (2023). Blockchain-enabled carbon and energy trading for network-constrained coal mines with uncertainties. *IEEE Trans. Sustain. Energy* 14 (3), 1634–1647. doi:10.1109/TSTE.2023.3240203
- Jiang, Y., Ren, Z., and Li, W. (2024). Committed carbon emission operation region for integrated energy systems: concepts and analyses. *IEEE Trans. Sustain. Energy* 15 (2), 1194–1209. doi:10.1109/TSTE.2023.3330857
- Kong, A., Li, C., Chen, L., Zhu, X., and Xu, X. (2020). "ADMM-based distributed optimal dispatch of integrated energy system considering uncertainties of source and load," in 2020 IEEE sustainable power and energy conference (ISPEC), Chengdu, China, 23–25 November 2020 (IEEE), 1222–1227. doi:10.1109/ISPEC50848.2020.9351300
- Li, J., Fang, Z., Wang, Q., Zhang, M., Li, Y., and Zhang, W. (2024). Optimal operation with dynamic partitioning strategy for centralized shared energy storage station with integration of large-scale renewable energy. *J. Mod. Power Syst. Clean Energy* 12 (2), 359–370. doi:10.35833/MPCE.2023.000345
- Lu, X., Zhong, Z., Xue, X., Wu, Y., Ai, X., and Fang, J. (2022). "Optimal real-time operation strategy of microgrid with power-to-hydrogen device: an ADP approach," in 2022 5th international conference on energy, electrical and power engineering (CEEPE), Chongqing, China, 22–24 April 2022 (IEEE), 758–763. doi:10.1109/CEEPE55110.2022.9783327
- Pan, B., Tian, Y., Chen, K., Li, W., and Tang, X. (2022). "Distributed operation strategy of electricity-gas integrated system based on improved ADMM," in 2022 12th international conference on power and energy systems (ICPES). Guangzhou, China, 23–25 December 2022 (IEEE), 310–314. doi:10.1109/ICPES56491.2022.10072950
- Pan, G., Hu, Q., Gu, W., Ding, S., Qiu, H., and Lu, Y. (2021). Assessment of plum rain's impact on power system emissions in Yangtze-Huaihe River basin of China. *Nat. Commun.* 12 (6156), 6156. doi:10.1038/s41467-021-26358-w
- Wu, Y., Yao, L., Liao, S., and Mao, B. (2021). "Distributed optimal scheduling of integrated energy system based on ADMM algorithm," in 2021 IEEE sustainable power and energy conference (ISPEC). Nanjing, China, 23–25 December 2021 (IEEE), 902–906. doi:10.1109/ISPEC53008.2021.9736049
- Zhang, R., Chen, Y., Li, Z., Jiang, T., and Li, X. (2024). Two-stage robust operation of electricity-gas-heat integrated multi-energy microgrids considering heterogeneous uncertainties. *Appl. Energy* 371 (123690), 123690. doi:10.1016/j.apenergy.2024.123690
- Zhao, F., Li, Y., Wei, Y., Wang, D., Li, F., and Yang, X. (2022). "Integrated energy production unit capacity optimization and year-round operation simulation," in 2022 7th international conference on power and renewable energy (ICPRE). Shanghai, China, 23–26 September 2022 (IEEE), 1206–1210. doi:10.1109/ICPRE55555.2022.9960424
- Zhuang, W., Pan, G., Gu, W., Zhou, S., Hu, Q., Gu, Z., et al. (2023). Hydrogen economy driven by offshore wind in regional comprehensive economic partnership members. *Energy & Environ. Sci.* 16 (5), 2014–2029. doi:10.1039/D2EE02332F

Publisher's note

All claims expressed in this article are solely those of the authors and do not necessarily represent those of their affiliated organizations, or those of the publisher, the editors and the reviewers. Any product that may be evaluated in this article, or claim that may be made by its manufacturer, is not guaranteed or endorsed by the publisher.

Nomenclature

Abbreviations	
PV	Photovoltaic generator
WT	Photovoltaic generator
CHP	Combines heat and power
GB	Gas boiler
EH	Electric heater
EC	Electrolytic cell
FC	Fuel cell
MR	Methanator
BT	Battery
HC	Heat storage tank
HS	Hydrogen storage tank
GS	Gas storage tank
EL	Electric load
HL	Heating load
HGL	Hydrogen load
Parameters	
IMG	The number of micro-energy grids
T	Length of scheduling period
K	Types of EC and FC
Δt	Scheduling time resolution
$c_{PV,om}^{i,t} / c_{WT,om}^{i,t}$	Cost coefficient of PV and WT
$c_{CHP,om}^{i,t} / c_{FC,om}^{i,k,t}$	Cost coefficient of CHP and FC
$c_{EC,om,1}^{i,k,t} / c_{EC,om,2}^{i,k,t}$	Cost coefficient 1/2 of EC
$c_{EH,om}^{i,t} / c_{GB,om}^{i,t} / c_{MR,om}^{i,t}$	Cost coefficient of EH, GB and MR
$c_{BT/HC/HS/GS,om}^{i,t}$	Cost coefficient of BT/HC/HS/GS
$R_{FU}^{i,t} / H_{FU}^{i,t}$	The natural gas price and natural gas calorific value
$c_{EX}^{i,j,t}$	Electricity purchase price from other micro-energy grids
$c_{GD,b}^{i,t} / c_{GD,s}^{i,t}$	Electricity purchase/sell price from/to the power grid
$P_{GD,b,min}^{i,t} / P_{GD,b,max}^{i,t}$	The minimum/maximum power purchased from the power grid
$P_{GD,s,min}^{i,t} / P_{GD,s,max}^{i,t}$	The minimum/maximum power sold to the power grid
$P_{gas,b,min}^{i,t} / P_{gas,b,max}^{i,t}$	The minimum/maximum power purchased from the gas company
$\eta_{CHP,E}^{i,t} / \eta_{FC,E}^{i,k,t}$	The power generation efficiency of CHP/FC
$V_{CHP}^{i,t} / V_{FC}^{i,k,t}$	Thermoelectric ratio of CHP/FC
$\eta_{EC}^{i,k,t} / \eta_{EH}^{i,t}$	The efficiency of EC/EH
$\eta_{GB}^{i,t} / \eta_{MR}^{i,t}$	The efficiency of GB/MR
Cap_{PV}^i / Cap_{WT}^i	Installed capacity of PV/WT
$Cap_{CHP,E}^i / Cap_{FC,E}^{i,k}$	Installed capacity of CHP/FC
Cap_{EC}^i / Cap_{EH}^i	Installed capacity of EC/EH
Cap_{GB}^i / Cap_{MR}^i	Installed capacity of GB/MR
$\delta_{PV,fore}^{i,t} / \delta_{WT,fore}^{i,t}$	The ratio of the predicted output power to the installed capacity of PV and WT
$\delta_{CHP,out,E,min}^{i,t} / \delta_{CHP,out,E,max}^{i,t}$	The ratio of the minimum/maximum output power to the installed capacity of CHP
$\delta_{FC,out,E,min}^{i,k,t} / \delta_{FC,out,E,max}^{i,k,t}$	The ratio of the minimum/maximum output power to the installed capacity of FC
$\delta_{EC,out,min}^{i,t} / \delta_{EC,out,max}^{i,t}$	The ratio of the minimum/maximum output power to the installed capacity of EC
$\delta_{EH,out,min}^{i,t} / \delta_{EH,out,max}^{i,t}$	The ratio of the minimum/maximum output power to the installed capacity of EH
$\delta_{GB,out,min}^{i,t} / \delta_{GB,out,max}^{i,t}$	The ratio of the minimum/maximum output power to the installed capacity of GB
$\delta_{MR,out,min}^{i,t} / \delta_{MR,out,max}^{i,t}$	The ratio of the minimum/maximum output power to the installed capacity of MR
$\delta_{CHP,ramp,max}^{i,t} / \delta_{FC,ramp,max}^{i,k} / \delta_{EC,ramp,max}^{i,k}$	The ratio of the maximum ramping power to the installed capacity of CHP/FC/EC
$\eta_{BT/HC/HS/GS,c}^{i,t} / \eta_{BT/HC/HS/GS,d}^{i,t}$	The charging/discharging efficiency of BT/HC/HS/GS
$\delta_{BT/HC/HS/GS,c,min}^{i,t} / \delta_{BT/HC/HS/GS,c,max}^{i,t}$	The ratio of the minimum/maximum charging power to the installed capacity of BT/HC/HS/GS
$\delta_{BT/HC/HS/GS,d,min}^{i,t} / \delta_{BT/HC/HS/GS,d,max}^{i,t}$	The ratio of the minimum/maximum discharging power to the installed capacity of BT/HC/HS/GS
$v_{BT/HC/HS/GS,min}^{i,t} / v_{BT/HC/HS/GS,max}^{i,t}$	The ratio of the minimum/maximum energy stored to the installed capacity of BT/HC/HS/GS
$\sigma_{BT/HC/HS/GS}^i$	Self-discharge rate of BT/HC/HS/GS
$\delta_{EC,in,1,min}^{i,k} / \delta_{EC,in,1,max}^{i,k}$	The ratio of the minimum/maximum input power to the installed capacity of EC
$\delta_{EC,boot}^{i,k}$	The ratio of the startup power to the installed capacity of EC
$y_{EC,max}^{i,k} / z_{EC,max}^{i,k}$	The maximum startup/shut down times of EC within a typical day
$P_{EX,min}^{i,j,t} / P_{EX,max}^{i,j,t}$	The minimum/maximum exchanged power with other micro-energy grids
$A_{EX}^{i,j,t}$	The connection topology between micro-energy grids
Variables	
$P_{PV,out}^{i,t} / P_{WT,out}^{i,t}$	The output power of PV and WT
$P_{CHP,in}^{i,t} / P_{CHP,out,E}^{i,t} / P_{CHP,out,H}^{i,t}$	The input/output electric/output thermal power of CHP
$P_{FC,in}^{i,k,t} / P_{FC,out,E}^{i,k,t} / P_{FC,out,H}^{i,k,t}$	The input/output electric/output thermal power of FC
$P_{EC,in,1}^{i,k,t} / P_{EC,in,2}^{i,k,t} / P_{EC,out}^{i,k,t}$	The input 1/input 2/output power of EC
$P_{EH,in}^{i,t} / P_{EH,out}^{i,t}$	The input/output power of EH

$P_{GB,in}^{i,t} / P_{GB,out}^{i,t}$	The input/output power of GB
$P_{MR,in}^{i,t} / P_{MR,out}^{i,t}$	The input/output power of MR
$P_{GD,b}^{i,t} / P_{GD,s}^{i,t}$	The purchased/sold power from/to the power grid
$x_{GD,b}^{i,t} / x_{GD,s}^{i,t}$	The purchased/sold status from/to the power grid, 0-1 variable
$P_{gas,b}^{i,t}$	The purchased gas power from the gas company
$P_{BT/HC/HS/GS,c}^{i,t} / P_{BT/HC/HS/GS,d}^{i,t}$	The charge/discharge power of BT/HC/HS/GS
$P_{BT/HC/HS/GS,c,EX}^{i,t} / P_{BT/HC/HS/GS,d,EX}^{i,t}$	The charge/discharge power of BT/HC/HS/GS exchanged with micro-energy grids
$W_{BT/HC/HS/GS}^{i,t}$	The stored energy of BT/HC/HS/GS
$x_{BT/HC/HS/GS,c}^{i,t} / x_{BT/HC/HS/GS,d}^{i,t}$	The charge/discharge status of BT/HC/HS/GS, 0-1 variable
$x_{EC}^{i,k,t}$	The input/output exchanged power with other micro-energy grids
$y_{EC}^{i,k} / z_{EC}^{i,k}$	The start and stop actions of EC, 0-1 variable
$P_{EX,in}^{i,j,t} / P_{EX,out}^{i,j,t}$	The input/output exchanged power with other micro-energy grids
$x_{EX,in}^{i,j,t} / x_{EX,out}^{i,j,t}$	The input/output exchanged power status with other micro-energy grids, 0-1 variable